

Application of a new spectral theory of stably stratified turbulence to atmospheric boundary layers over sea ice

Semion Sukoriansky (semion@bgu.ac.il)

Department of Mechanical Engineering/Perlstone Center for Aeronautical Engineering Studies, Ben-Gurion University of the Negev, Beer-Sheva 84105, Israel

Boris Galperin (bgalperin@marine.usf.edu)

College of Marine Science, University of South Florida, St. Petersburg, Florida 33701, USA

Veniamin Perov (vperov@smhi.se)

Department of Research and Development, Swedish Meteorological and Hydrological Institute, SE-601 76 Norrköping, Sweden

December 17, 2004

Abstract. A new spectral closure model of stably stratified turbulence is used to develop a $K - \epsilon$ model suitable for applications to atmospheric boundary layers (ABLs). This $K - \epsilon$ model utilizes the vertical viscosity and diffusivity obtained from the spectral theory. In the ϵ -equation, the Coriolis parameter-dependent formulation of the coefficient C_1 suggested by Detering and Etling is generalized to include the dependence of the Brunt-Väisälä frequency, N . The new $K - \epsilon$ model is tested in simulations of ABLs over sea ice and compared with the data from BASE as simulated in LES by Kosovic and Curry and data from SHEBA.

Keywords: Turbulence, Spectral theories, Stable stratification, Atmospheric boundary layers

1. Introduction

Atmospheric boundary layers (ABLs) are the medium moderating between the atmosphere and the underlying surface. The physical processes in ABLs determine the surface fluxes of the momentum, temperature and humidity that are among the primary governors of the atmospheric and oceanic circulations on synoptic and global scales. Turbulence in ABL flows is strongly affected by density stratification. The subject of this paper are ABLs with stable stratification, or SBLs. Stable stratification tends to reduce the vertical mixing leading to the development of spatial anisotropy. With increasing strength of stratification, the near-surface layer may become pinched-off from the overlying circulation, essentially shielding this circulation from the surface fluxes. Referring to this phenomenon, (Mahrt, 1998; Mahrt, 1999) considered two prototype flow regimes, very stable and weakly stable, noting that in most cases, SBL flows are between these two ex-



© 2004 Kluwer Academic Publishers. Printed in the Netherlands.

tremes. The physics of the very stable SBLs are quite subtle. Although such SBLs become very shallow, down to 10 m or less (Kitaigorodskii and Joffre, 1988; King, 1990; Zilitinkevich and Mironov, 1996; Zilitinkevich et al., 2002a; Zilitinkevich and Baklanov, 2002; Zilitinkevich and Esau, 2002; Zilitinkevich and Esau, 2003), they still maintain well-developed turbulence (e.g., Larsen, 1990). Further analysis reveals that the effect of a very strong negative buoyancy force is two-fold. On the one hand, it tends to suppress vertical mixing; on the other, it enhances vertical velocity gradient thus increasing the velocity shear and the production of the turbulent kinetic energy. These opposing actions greatly enhance the irregularity of the flow field and its intermittency. This picture is further complicated by the contribution from internal waves and their breaking (Zilitinkevich, 2002). Similar phenomena are also observed in oceanic mixed layers with strong stable stratification where levels of turbulent energy and vertical eddy viscosity remain finite even for relatively large values of the Richardson number Ri (Peters et al., 1988, Cane, 1993).

Generally, spatial anisotropy and turbulence-internal wave interaction, features characteristic of stably stratified flows, are among the processes that are least friendly to mathematical modeling. Both phenomena are governed by strong nonlinearity and are not readily amenable to treatment within analytical theories. Therefore, most models either ignore these phenomena or include them using ad hoc approximations. Modeling of SBLs presents a challenge not only to the widely used Reynolds-averaged Navier-Stokes equations-based models (RANS) but also to large eddy simulations (LES) because strong stratification may have significant impact upon the subgrid-scale (SGS) modes; realistic SGS parameterizations must account for this effect.

Turbulence parameterizations used in atmospheric SBL and ocean circulation models are usually based on closure assumptions introduced in simple, nearly isotropic flows and extrapolated into real flows with strong anisotropy and waves. However, such extrapolation may take the closure models beyond their realm of applicability, degrading the quality of their predictive skills. Therefore, the improvement of the RANS models is an ongoing effort. Along with the RANS, alternative turbulence closure models have been developed during the recent decades. One class of such models is based upon spectral closure methods (McComb, 1991). Generally, spectral closures are more complicated than RANS models but to their advantage, they retain more comprehensive physics and are believed to be more accurate and general than their RANS counterparts. Spectral models have been widely used in analytical theories of turbulence as well as in Large Eddy Simulations (LES) (Galperin and Orszag, 1993). Recently, we have developed a

new spectral closure model based upon a mapping of the velocity field onto a quasi-Gaussian field whose modes are governed by the Langevin equation (Sukoriansky et al., 2003). The parameters of the mapping are calculated using a systematic process of successive averaging over small shells of velocity and temperature modes that yields equations for increasingly larger-scale modes. In this procedure, the combined contribution of turbulence and internal waves is accounted for and the spatial anisotropy is explicitly resolved (Sukoriansky and Galperin, 2004). When the process of successive averaging is extended to the largest scales available in the system (i.e., the turbulence macroscale), the spectral closure yields a new RANS model. This model has been implemented as a new version of the $K - \epsilon$ model and tested in single-column simulations of SBLs over sea ice. Two test cases, the Beaufort Arctic Storms Experiment (BASE) and the Surface Heat Budget in the Arctic program (SHEBA), were selected. This selection was stipulated, on the one hand, by the fact that the data included cases of moderate and strong stable stratification such that the new model could be put through a severe testing; on the other, the data has been replicated in LES by Kosovic and Curry (2000) which, thus, could be used as a benchmark for simulations with the new $K - \epsilon$ model. This paper describes the results of these simulations. The next section provides a brief outlook of the spectral closure theory utilized in this study while a subsequent section elaborates on the implementation of this theory in $K - \epsilon$ modeling. In Section 4, results of simulations with the new $K - \epsilon$ model are compared with the LES of BASE and with the data from SHEBA. Finally, Section 5 provides discussion and conclusions.

2. The spectral closure model

The spectral closure theory is developed for a fully three-dimensional, incompressible, turbulent flow field with an imposed homogeneous, vertical, stable temperature gradient; the flow is governed by the momentum, temperature and continuity equations in Boussinesq approximation,

$$\frac{\partial \mathbf{u}}{\partial t} + (\mathbf{u} \nabla) \mathbf{u} + \alpha g \theta \hat{e}_3 = \nu_0 \nabla^2 \mathbf{u} - \frac{1}{\rho} \nabla P + \mathbf{f}^0, \quad (1)$$

$$\frac{\partial \theta}{\partial t} + (\mathbf{u} \nabla) \theta + \frac{d\Theta}{dz} u_3 = \kappa_0 \nabla^2 \theta, \quad (2)$$

$$\nabla \cdot \mathbf{u} = 0, \quad (3)$$

where \mathbf{u} and θ are the fluctuating velocity and the fluctuating potential temperature, respectively; P is the pressure, ρ is the constant reference

density, ν_0 and κ_0 are the molecular viscosity and diffusivity, respectively, α is the thermal expansion coefficient, g is the acceleration due to gravity directed downwards, $\frac{d\Theta}{dz}$ is the mean potential temperature gradient, and \mathbf{f}^0 represents a large-scale external energy source customarily used in spectral theories of turbulence; it maintains turbulence in statistically steady state and may originate from large-scale shear instabilities. According to the Kolmogorov theory of turbulence, the details of this forcing are immaterial in statistical description; its net effect is communicated to the fluid via a single integral parameter, the rate of the energy injection at large scales. Due to strong nonlinear interactions, the external forcing excites all Fourier modes down to the dissipative scale $k_d = (\epsilon/\nu_0^3)^{1/4}$ (ϵ is the rate of viscous dissipation). The modes exert indiscriminant, random agitation upon each other which is accompanied by simultaneous random damping. In statistically steady state, the processes of forcing and damping balance each other; in other words, every Fourier mode $\mathbf{u}(\mathbf{k}, \omega)$ (\mathbf{k} and ω being Fourier space wave number and frequency, respectively) receives and loses equal, in statistical sense, amounts of energy. Reflecting the duality between nonlinear interactions and stochastic forcing and damping, the nonlinear term in Eq. (1) can be replaced by a random, *modal* forcing \mathbf{f} and damping represented by turbulent viscosity. The resulting linear equation with stochastic forcing and damping is known as the Langevin equation,

$$u_i(\mathbf{k}, \omega) = G_{ij}(\mathbf{k}, \omega) f_j(\mathbf{k}, \omega). \quad (4)$$

In the characterization by Kraichnan (1987), the Langevin equation can be viewed as a device that facilitates the replacement of the original nonlinear Navier-Stokes equation by a linear, forced, stochastic equations in which the energy budget is systematically adjusted for every Fourier mode. For the temperature, a similar Langevin-type equation can be derived; it can be shown that the role of the random forcing in this case is assumed by the vertical velocity fluctuation (Sukoriansky and Galperin, 2004),

$$\theta(\mathbf{k}, \omega) = -\frac{d\Theta}{dz} G_\theta(\mathbf{k}, \omega) u_3(\mathbf{k}, \omega). \quad (5)$$

The major closure assumption of the theory is that the forcing \mathbf{f} is quasi-Gaussian, placing the present spectral theory in the family of the classical quasi-Gaussian spectral closures such as the direct interaction approximation (DIA) (Kraichnan, 1959); the eddy-damped, quasi-normal, Markovian approximation (EDQNM) (Orszag, 1977), or, collectively, the renormalized perturbation theories (RPT) (McComb, 1991). This assumption enables one to derive expressions for the eddy

viscosity and eddy diffusivity. The fluctuating velocity field is zero-mean and incompressible imposing the same restraints upon the forcing $\mathbf{f}(\mathbf{k}, \omega)$ in (4); in the assumption of quasi-Gaussianity, this forcing is fully determined by its two-point, two-time correlation function. The choice of the analytical representation of this correlation function is guided by general considerations of spatial and temporal homogeneity and incompressibility which almost completely determine its functional form (Sukoriansky et al., 2003). By its physical meaning, the correlation function of the forcing $\mathbf{f}(\mathbf{k}, \omega)$ accounts for the statistical mean energy input to a given mode k via its interaction with all other modes such that its amplitude, D , is proportional to the mean rate of energy transfer through that mode. The balance between the energy gain due to the eddy forcing and the energy loss due to the eddy damping enables one to relate the forcing amplitude D to the dissipation rate ϵ and the buoyancy destruction. In the case of neutral stratification, this approach recovers some basic features of isotropic homogeneous turbulence including the Kolmogorov spectrum and the Kolmogorov constant (Sukoriansky et al., 2003; Yakhot and Orszag, 1986).

Rigorous derivation of the velocity and temperature response, or Green functions, $G_{ij}(\mathbf{k}, \omega)$ and $G_\theta(\mathbf{k}, \omega)$, from the original system (1-3) is given in Sukoriansky and Galperin (2004); here, only their final representation is shown:

$$G_{ij}(\mathbf{k}, \omega) = G(\mathbf{k}, \omega) [\delta_{ij} + A(\mathbf{k}, \omega)P_{i3}(\mathbf{k})\delta_{j3}], \quad (6)$$

$$A(\mathbf{k}, \omega) = \frac{-N^2}{(-i\omega + \nu_h k_h^2 + \nu_z k_z^2)(-i\omega + \kappa_h k_h^2 + \kappa_z k_z^2) + N^2 P_{33}(\mathbf{k})}, \quad (7)$$

$$G(\mathbf{k}, \omega) = \left(-i\omega + \nu_h k_h^2 + \nu_z k_z^2\right)^{-1}, \quad (8)$$

$$G_\theta(\mathbf{k}, \omega) = \left(-i\omega + \kappa_h k_h^2 + \kappa_z k_z^2\right)^{-1}, \quad (9)$$

where k_h and k_z are the horizontal and vertical wave numbers; ν_h, κ_h and ν_z, κ_z are the horizontal and vertical eddy viscosities and diffusivities, respectively; $N \equiv \sqrt{\alpha g(d\Theta/dz)}$ is the Brunt-Väsälä frequency; δ_{ij} is the Kronecker delta-symbol, and $P_{ij}(\mathbf{k}) = \delta_{ij} - k_i k_j / k^2$.

Note that due to the effect of stable stratification, the Green's function $G_{ij}(\mathbf{k}, \omega)$ has acquired tensorial properties, while eddy viscosities and diffusivities became different in the vertical and in the horizontal. Expression (7) contains complex poles generated by the term $N^2 P_{33}(\mathbf{k})$ in its denominator. The real part of these poles yields a dispersion relation for internal waves in the presence of turbulence (Sukoriansky

and Galperin, 2004),

$$\omega^2 = \omega_0^2 \left\{ 1 - \left(\frac{k}{k_O} \right)^{4/3} \left[\frac{\left(\frac{\kappa_z}{\nu_n} - \frac{\nu_z}{\nu_n} \right) \cos^2 \theta + \left(\frac{\kappa_h}{\nu_n} - \frac{\nu_h}{\nu_n} \right) \sin^2 \theta}{4 \sin \theta} \right]^2 \right\}, \quad (10)$$

where

$$\omega_0^2 = N^2 \sin^2 \theta \quad (11)$$

is the classical dispersion relation for linear internal waves. Here, θ is the angle between the vector \mathbf{k} and the vertical axis; $k_O = (N^3/\epsilon)^{1/2}$ is the Ozmidov wave number, and ν_n is the eddy viscosity in the case of neutral stratification. The expression in the figure brackets of Eq. (10) describes internal wave frequency shift due to turbulence. In the limit $k/k_O \rightarrow 0$ (large scales; strong stratification), the classical dispersion relation (11) is recovered. On the other hand, on small scales, $k/k_O \rightarrow \infty$, the increasingly disorganizing action of the turbulent overturn eventually overwhelms internal waves rendering the flow field purely turbulent. The threshold of the internal waves generation in the presence of turbulence is given by $\omega = 0$ which, using Eq. (10), yields

$$k_t = k_O \left| \frac{4 \sin \theta}{\left(\frac{\kappa_z}{\nu_n} - \frac{\nu_z}{\nu_n} \right) \cos^2 \theta + \left(\frac{\kappa_h}{\nu_n} - \frac{\nu_h}{\nu_n} \right) \sin^2 \theta} \right|^{3/2}. \quad (12)$$

Assuming that the wave radiation begins at relatively large k , at which turbulence is still close to isotropic, the following estimates can be made: $\kappa_z/\nu_n - \nu_z/\nu_n \approx 0.4$; $\kappa_h/\nu_n - \nu_h/\nu_n \approx 0.4$ (Sukoriansky and Galperin, 2004) yielding

$$k_t \simeq k_O |10 \sin \theta|^{3/2} \simeq 32 k_O |\sin \theta|^{3/2}. \quad (13)$$

Thus, the internal gravity waves exist only at wave numbers k smaller than the threshold value k_t .

The parameters of eddy damping are calculated using a systematic algorithm of successive averaging over small shells of velocity and temperature modes which, utilizing the Langevin equations (4) and (5), yields small increments to the vertical and horizontal viscosities and diffusivities. The details of this calculation are described in Sukoriansky and Galperin (2004); it leads to a system of four coupled ODEs for $\nu_h, \nu_z, \kappa_h, \kappa_z$,

$$\frac{d}{dk}(\nu_h, \nu_z, \kappa_h, \kappa_z) = -C \frac{\epsilon}{k^5} R_{1,2,3,4}(\nu_h, \nu_z, \kappa_h, \kappa_z), \quad (14)$$

where $C \simeq 0.7$ and R_1 through R_4 are transcendental expressions (Sukoriansky and Galperin, 2004). These expressions are given in the

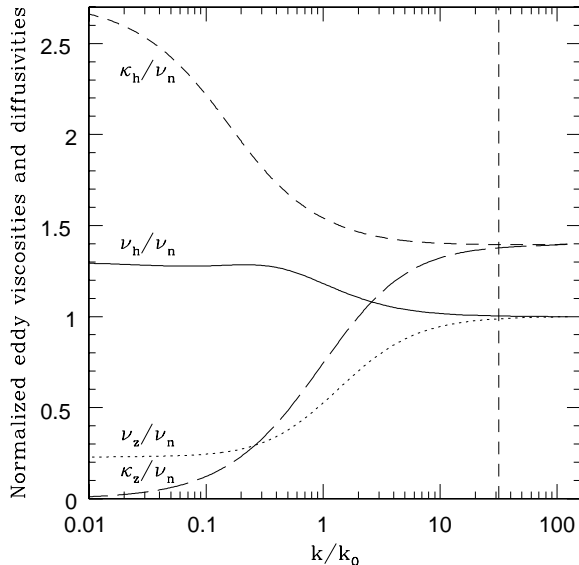


Figure 1. Normalized horizontal and vertical eddy viscosities and diffusivities as functions of k/k_0 . The vertical dashed line shows the location of k_t , the threshold of internal wave generation in presence of turbulence.

Appendix for the asymptotic cases of weak and strong stratification. The computation of the viscosities and diffusivities starts at the Kolmogorov scale k_d where the initial values of ν_z and κ_z are equal to their respective molecular values ν_0 and κ_0 and is continued to an arbitrary wave number $k < k_d$. The system (14) can only be solved numerically. Solutions obtained for the nondimensional variables ν_h/ν_n , ν_z/ν_n , κ_h/ν_n and κ_z/ν_n are presented on Fig. 1 as functions of the ratio k/k_0 .

At large k/k_0 (relatively small scales), as expected, all the nondimensional parameters approach the values typical of the case of neutral stratification. At small k/k_0 , on the other hand, approximately at the threshold of internal wave generation, horizontal and vertical viscosities and diffusivities depart markedly. Horizontal viscosity increases by a factor of 1.3 compared to the neutral case, while vertical viscosity decreases to approximately 1/6 of the horizontal viscosity value. The vertical viscosity ν_z preserves a finite asymptotic value even for very strong stable stratification. This “residual” momentum mixing may be due to the action of internal waves which are the integral part of the present spectral model. It is worth of noting that the onset of internal wave radiation is concurrent with the emergence of flow anisotropy

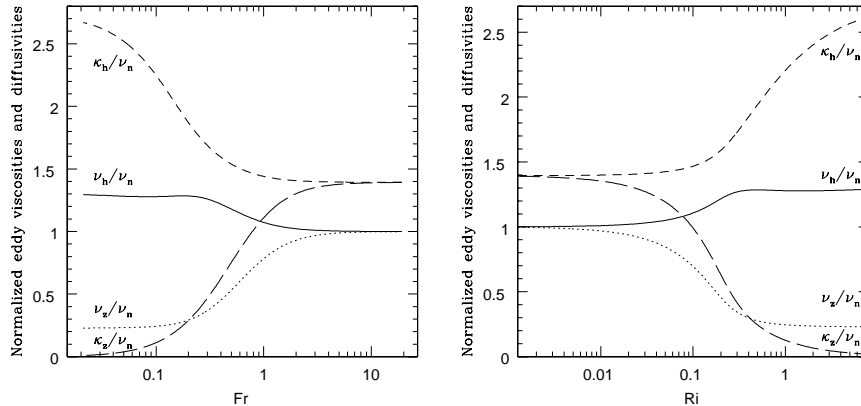


Figure 2. Normalized turbulent exchange coefficients as functions of the Froude number Fr (left panel) and the gradient Richardson number Ri (right panel).

induced by stable stratification and the beginning of strong deviations in eddy viscosities and diffusivities from their values in the neutral case.

Another interesting result is that $\kappa_z/\kappa_h \rightarrow 0$ for $k/k_O \rightarrow 0$; under strong stratification, vertical diffusivity is suppressed while its horizontal counterpart is enhanced almost by a factor of 3 compared to the neutral case. Flows of this kind may reveal certain features of two-dimensional (2D) turbulence (Cho et al., 1999).

The new spectral model can be used for simulations of turbulent shear flows with stable stratification. The scale-dependent viscosities and diffusivities can be utilized for derivation of the respective subgrid-scale (SGS) parameters in LES. Let us denote the wave number of LES grid resolution by k_c . In many SGS parameterizations in use today, the effect of stable stratification is not taken into account. Figure 1 provides a criterion when such an assumption is acceptable. Namely, for $k_c > k_t$, k_t is given by Eq. (13), the effect of stable stratification is small such that the eddy viscosity and eddy diffusivity can be taken the same as in the case of neutral stratification. However, for $k_c < k_t$, the effect of stable stratification cannot be neglected; furthermore, it profoundly increases with decreasing ratio k_c/k_t . The need to improve SGS representation for LES of strongly stratified flows was emphasized in the recent GABLS report (Holtslag, 2003). The present theory provides a self-consistent framework to address this need.

The process of small scales elimination can be extended to the largest scale of turbulence identified with the integral length scale, k_L^{-1} . This approach is analogous to the Reynolds averaging and the resulting equations represent a sort of a RANS model. In the RANS format, the

non-dimensional eddy viscosities and eddy diffusivities, ν_h/ν_n , ν_z/ν_n , κ_h/ν_n and κ_z/ν_n , become functions of k_L/k_O . It is well known in the $K-\epsilon$ modeling that k_L is related to the total kinetic energy of the flow, K , as $k_L \propto \epsilon/K^{3/2}$, such that $k_L/k_O \propto Fr^{3/2}$, where $Fr = \epsilon/KN$ is the Froude number. The dependence of the eddy viscosities and eddy diffusivities on Fr is shown on Fig. 2; more detailed derivations are given in Sukoriansky and Galperin (2004). Alternatively, these parameters can be represented as functions of the gradient Richardson number, $Ri = N^2/S^2$. This can be done by introducing a closure assumption that prescribes an equilibrium between the sum of the rate of the energy dissipation, ϵ , and the buoyancy destruction, B ($B = \kappa_z N^2$), with the shear production, P ($P = \nu_z S^2$, S is the magnitude of the shear). The Ri -dependent non-dimensional eddy viscosities and eddy diffusivities are also shown on Fig. 2. By virtue of derivation, the major features of the dependence on Fr and on Ri , shown in Fig. 2, replicate those of the dependence on k/k_O shown in Fig. 1. Turbulent viscosities and diffusivities begin to depart from their values under neutral stratification at relatively small Ri and large Fr . The most significant change in their values takes place in the range of Fr and Ri between 0.1 and 1; however, the spectral theory does not predict a single value of the critical Richardson number, such as 1/4 according to Miles (1961) and Howard (1961) or 1 according to Abarbanel et al. (1984), at which turbulent mixing ceases completely. For $Fr < 1$ and $Ri > 0.1$, both vertical viscosity and diffusivity decrease with diffusivity decreasing faster. Eventually, stable stratification may totally suppress vertical scalar mixing while vertical momentum mixing continues even at relatively high Ri , apparently, due to the contribution of internal waves. Such behavior is not easily reproduced in RANS models or in second-moment closure models in use in atmospheric or oceanographic modeling where the concept of externally imposed “residual” mixing has been routinely utilized to account for otherwise suppressed turbulent mixing (Kantha and Clayson, 1994; Large et al., 1994). This result is consistent with the atmospheric and oceanic data mentioned in the Introduction that pointed out to turbulence survival in flows with very strong stable stratification. Recent towed chain observations in the ocean (Mack and Schoeberlein, 2004) are also supportive of the gradual attenuation of turbulence under the action of increasing stable stratification, rather than a sharp cut-off: “... no single critical 10-m Ri , either 0.25 (Miles and Howard) or 1 (Abarbanel et al.), is identified.”

One of the important characteristics of stably stratified turbulent flows is the behavior of the “vertical” turbulent Prandtl number, $Pr_t = \nu_z/\kappa_z$, as a function of Ri . Figure 3 compares the prediction of the

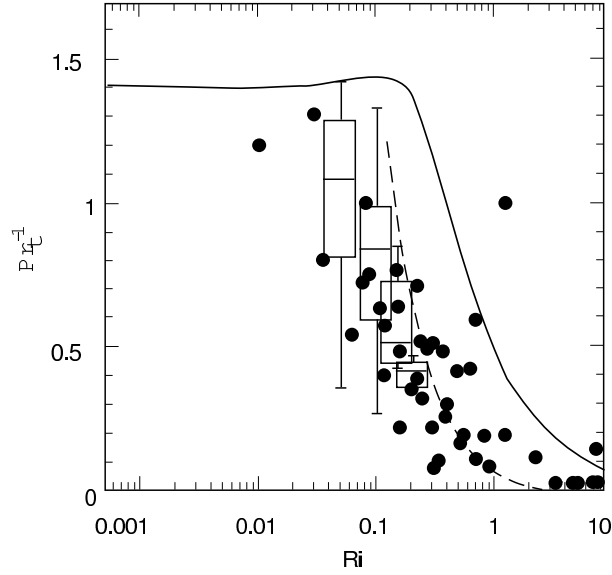


Figure 3. Inverse turbulent Prandtl number, Pr_t^{-1} , as a function of Ri . Data points are the observations by Kondo et al., 1978; long-dashed line refers to the model by Zilitinkevich and Calanca (2000), the solid line is the present spectral theory.

present model with the observational data from Kondo et al. (1978) and a model by Zilitinkevich and Calanca (2000).

Although the general trend of Pr_t^{-1} is reproduced well for all Ri , the theoretical values are somewhat higher than the data. Note that partially, this is due to the uncertainty with the value of Pr_{t0} in neutral stratification. In the present model, $Pr_{t0} = 0.72$; however, this value may vary between about 0.5 and 1.2 which would affect the rest of the curve. The broad range of variation of Pr_t^{-1} in the data points out to a need for further experimental research in order to reduce the noise-to-signal ratio.

3. Implementation of the spectral results in $K - \epsilon$ modeling of SBLs

The RANS models are concerned with the equations for mean horizontal velocities U and V and mean potential temperature Θ (PT). In applications to ABLs, they employ turbulent viscosity and diffusivity, K_M and K_H . The central problem of the RANS modeling is the derivation of the appropriate expressions for K_M and K_H . In a standard $K - \epsilon$ model used in neutrally stratified flows, the values of K_M and K_H are

calculated using the well-known Kolmogorov-Prandtl formulation,

$$K_M = C_\mu \frac{K^2}{\epsilon}, \quad K_H = Pr_{t0}^{-1} C_\mu \frac{K^2}{\epsilon}, \quad (15)$$

where the coefficient C_μ is constant and equal to 0.09 (Rodi, 1980). A similar value was obtained within the present spectral theory (Sukoriansky and Galperin, 2004). In the format of $K - \epsilon$ modeling, the turbulent kinetic energy K and the dissipation rate ϵ are obtained from additional prognostic equations. In neutral stratification, $K - \epsilon$ modeling has been well established and widely used. When the stratification is not neutral, the $K - \epsilon$ equations in 1D, single-column formulation take the form

$$\begin{aligned} \frac{DK}{Dt} &= K_M \left[\left(\frac{\partial U}{\partial z} \right)^2 + \left(\frac{\partial V}{\partial z} \right)^2 \right] - \frac{g}{\Theta_0} K_H \frac{\partial \Theta}{\partial z} \\ &\quad - \epsilon + \frac{\partial}{\partial z} \left(K_q \frac{\partial K}{\partial z} \right), \end{aligned} \quad (16)$$

$$\begin{aligned} \frac{D\epsilon}{Dt} &= \frac{\epsilon}{K} \left\{ C_1 K_M \left[\left(\frac{\partial U}{\partial z} \right)^2 + \left(\frac{\partial V}{\partial z} \right)^2 \right] - C_3 \frac{g}{\Theta_0} K_H \frac{\partial \Theta}{\partial z} \right\} \\ &\quad - C_2 \frac{\epsilon^2}{K} + \frac{\partial}{\partial z} \left(K_\epsilon \frac{\partial \epsilon}{\partial z} \right). \end{aligned} \quad (17)$$

The terms on the right side of Eq. (16) represent shear production, buoyant destruction, dissipation and vertical turbulent transport of K . The terms on the right side of Eq. (17) are shear and buoyancy forcing, destruction, and vertical turbulent transport of ϵ . In addition to the conventional vertical eddy viscosity and diffusivity, K_M and K_H , respectively, Eqs. (16,17) also involve vertical turbulent mixing coefficients for the turbulence kinetic energy and dissipation, K_q and K_ϵ , which, following Rodi (1980), have been set to $K_q = K_M/\sigma_q$ and $K_\epsilon = K_M/\sigma_\epsilon$, where $\sigma_q = 1.0$ and $\sigma_\epsilon = 1.3$. The coefficients C_1 , C_2 and C_3 are constants in a standard $K - \epsilon$ model. Following Rodi (1980), their values are $C_1 = 1.44$ and $C_2 = 1.92$ in neutral flows. When stratification is not neutral, the value of C_3 is customarily set at 1.

In stratified flows, the $K - \epsilon$ formulation is affected in two aspects: (i) the coefficient C_μ in (15) is multiplied by a non-dimensional function of stratification (the so-called stability function), and (ii) the coefficients C_1 , C_2 and C_3 in the ϵ -equation may also become flow-dependent. In dealing with (i), the vertical turbulent viscosity and diffusivity, K_M and K_H , can be determined from a Reynolds stress model in which closure assumptions are invoked for all components of the Reynolds stress tensor and the heat flux vector. A well-known Reynolds stress model widely used in meteorological and oceanographic applications is the Mellor-Yamada (MY) model and its modifications (Mellor and Yamada, 1982;

Galperin et al., 1988; Galperin and Kantha, 1989; Galperin et al., 1989; Galperin and Mellor, 1991; Kantha and Clayson, 1994, Kantha, 2003). Although the MY model employs prognostic equation for Kl rather than ϵ (l being the turbulence macroscale), the dissipation equation can readily be implemented in that scheme. The aspect (ii) is more difficult to tackle because the ϵ -equation, as well as its MY counterpart, the Kl equation, are not derived from any conservation law and merely follow the pattern of the turbulent energy equation (16). The problematic issues of the ϵ -equation have been thoroughly discussed in the literature and will not be repeated here. Both the Reynolds stress models and the ϵ -equation have problems in stratified ABLs. For instance, the MY models have too low values of the critical Richardson numbers at which the vertical turbulent mixing is suppressed (Large et al., 1994; Cheng et al., 2002) while the standard $K - \epsilon$ model fails to replicate even a neutrally stratified ABLs (Detering and Etling, 1985).

In this paper, a new way of improving the $K - \epsilon$ models is suggested. The present spectral closure model is used to obtain the expressions for K_M and K_H thus circumventing certain shortcomings of the Reynolds stress modeling. It is hoped that the comprehensive physical foundation of the spectral model would ensure its better performance in situations where the Reynolds stress closures have difficulties.

The implementation of the new spectral model in the $K - \epsilon$ format suitable for 1D, single-column simulations of SBLs is straightforward. The vertical eddy viscosity and diffusivity coefficients predicted by the spectral model, namely ν_z and κ_z , are used in place of K_M and K_H . Utilizing the expression for the vertical viscosity in the neutral case,

$$\nu_n = C_\mu \frac{K^2}{\epsilon}, \quad (18)$$

where $C_\mu \simeq 0.09$, one can represent K_M and K_H as following:

$$K_M = \alpha_M C_\mu \frac{K^2}{\epsilon}, \quad K_H = \alpha_H C_\mu \frac{K^2}{\epsilon}, \quad (19)$$

where

$$\alpha_M = \frac{\nu_z}{\nu_n}, \quad \alpha_H = \frac{\kappa_z}{\nu_n} \quad (20)$$

are the aforementioned non-dimensional stability functions (note that Pr_{t0} in (19) is absorbed in α_H). These functions can be obtained from Fig. 2 in terms of the dependence on the Froude number, $Fr = \epsilon / KN$. Note that Fr is more general than Ri because the former can be used in shearless flows. In addition, the evaluation of Ri relies upon calculation of the gradients of U , V and Θ which may introduce significant numerical errors.

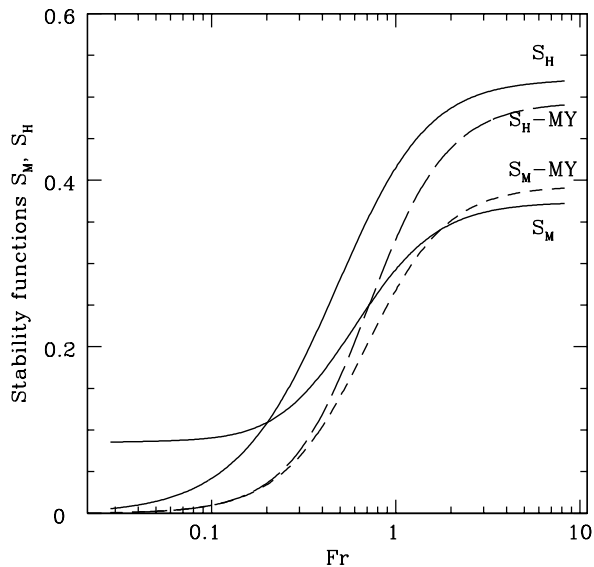


Figure 4. Comparison of stability functions calculated from the present model and from the MY model modified by Galperin et al. (1988).

It is of interest to compare functions α_M and α_H with respective stability functions in Reynolds stress closure models. For example, in MY models, eddy viscosity and eddy diffusivity are related to stability functions, S_M and S_H , as

$$K_M = qlS_M, \quad K_H = qlS_H, \quad (21)$$

where $q^2 = 2K$ (Mellor and Yamada, 1982; Galperin et al., 1988). Comparing (21) with (19) and using the MY relationship for the dissipation,

$$\epsilon = \frac{q^3}{B_1 l}, \quad (22)$$

where $B_1 = 16.6$ is one of the constants of the MY model, one obtains:

$$S_M = \left(\frac{B_1}{4}\right) C_\mu \alpha_M, \quad S_H = \left(\frac{B_1}{4}\right) C_\mu \alpha_H. \quad (23)$$

In Galperin et al. (1988), S_M and S_H were given as functions of $G_H = -(lN/q)^2$ which is related to the Froude number as $G_H = -(B_1 Fr/2)^{-2}$. Figure 4 compares stability functions obtained from the present spectral model with those from Galperin et al. (1988). A general observation is that with increasing stable stratification, both S_M and S_H in the MY model fall off quicker than their counterparts in the present spectral

model. The most significant difference is revealed in the behavior of S_M : in MY models, it becomes very small for $Fr < 0.2$ while in the spectral model, it remains finite even for very small values of Fr . The rapid decrease in S_M may be behind the well known deficiency of the MY models to often produce insufficient mixing in flows with strong stable stratification (e.g., Kantha, 2003). The spectral model appears to be free of this shortcoming.

Returning now to the dissipation equation, recall that when the coefficients C_1 , C_2 and C_3 are kept constant (the standard $K - \epsilon$ model), the model fails to replicate a neutrally-stratified ABL (Detering and Etling, 1985). Problems arising in applications of $K - \epsilon$ models to ABLs have been discussed elsewhere (Rodi, 1975; Rodi, 1980; Detering and Etling, 1985). It has been realized that the constants of a standard $K - \epsilon$ model are not universal and various ways have been proposed to make the constants flow-dependent. To achieve realistic description of the Leipzig velocity profile in neutral ABL, Detering and Etling (1985) have found it necessary to include the effect of the Earth's rotation in the ϵ -equation by making C_1 dependent on the friction velocity u_* and the Coriolis parameter f . Their modification can be expressed in terms of the friction velocity-based Rossby number $Ro_* = u_*/|f|L$,

$$C_1 = C_1^0 + C_f Ro_*^{-1}, \quad (24)$$

where C_1^0 is the standard coefficient equal to 1.44, $C_f = 111$ is an empirical constant and $L = 0.16K^{3/2}/\epsilon$ is the turbulence macroscale used in the $K - \epsilon$ modeling.

To include the effect of stable stratification, we have generalized Eq. (24) by adding a new term that depends on the friction velocity - based Froude number $Fr_* = u_*/NL$,

$$C_1 = C_1^0 + C_f Ro_*^{-1} - C_N Fr_*^{-1}, \quad (25)$$

where $C_N = 0.55$ is a new empirical constant. Taking into account that $f/N \sim 10^{-2}$ in off-equatorial regions, one can see that the rotation- and stratification-dependent terms in (25) are of the same order of magnitude. Note that a similar modification could be introduced in the coefficient C_3 rather than C_1 in which case the correction to $C_3^0 = 1$ would have a positive sign rather than the negative sign in (25). Here, however, it was preferred to associate all the corrections with one coefficient, C_1 , and to leave the other two coefficients intact. Also note that the formulation (25) is just a simple lowest order (linear) approximation to the function $C_1(Ro_*^{-1}, Fr_*^{-1})$. It is reasonable to assume that this lowest order approximation would not work at large Fr_*^{-1} . Indeed, it was found that a limitation

$$C_1 \geq C_1^0 \quad (26)$$

should be imposed on C_1 . Therefore, a more accurate functional form of C_1 could consist of the present formulation for small and very large Fr_*^{-1} , Eqs. (25) and (26), and some interpolating function for intermediate values of Fr_*^{-1} . However, the present formulation was found adequate for practical applications.

The $K - \epsilon$ model that includes prognostic equations (16) and (17) along with Eqs. (19), (20), (25) and (26) was implemented in the weather forecast model HIRLAM (High Resolution Limited Area Model) (Perov and Gollvik, 1996; Perov et al., 2001) and used to simulate SBL over sea ice. The results of these simulations are described in the next section.

4. Application of the new $K - \epsilon$ model to SBL over sea ice

Under the conditions of strong radiative cooling, the ABL over sea ice is normally clear and stably stratified. Such situation is common, for instance, in the Arctic during the winter. Several Arctic cloud climatologies indicate that at winter, clear-sky conditions are observed 40 - 60% of the time (Huschke, 1969; Hahn et al., 1984). During the Surface Heat Budget of the Arctic Ocean (SHEBA) experiment, clear-sky conditions were observed 27% of the winter time (Intrieri et al., 2002). The SBL over sea ice is of a special concern for numerical weather prediction and climate modeling because of the extremely cold temperatures in the winter Curry et al. (1996). The interest in SBLs over sea ice has also been stimulated by the recent attempts to interpret satellite data in situations where uncertainties in the remote sensing of sea ice lead to large discrepancies between surface- and satellite-derived climatologies (Rossow et al., 1993; Ramanathan et al., 1989). The properties of SBLs over ice have been studied by Tsay and Jayaweera (1984), Curry (1986), Curry et al. (1988), Fett et al. (1994), Ruffeaux et al. (1995) using the data collected during the Arctic Ice Dynamics Joint Experiment (AIDJEX, 1975) and the Arctic Stratus Experiment (1980). The Lead Experiment (LEADEX, 1992) was carried out to study interactions between ice field with leads and SBLs (Pinto and Curry, 1995; Walter et al., 1995). The autumnal freezing period has been studied during BASE (Paluch and Lenschow, 1997) and simulated in LES by Kosovic and Curry (2000). The Surface Heat Budget in the Arctic program (SHEBA, 1997-1998) was focused on surface fluxes at the sea ice during different seasons, particularly in the spring (Andreas et al., 1999). The LES results for BASE and data collected during the SHEBA campaign will be used for intercomparisons with the present $K - \epsilon$ model in a single-column format.

4.1. COMPARISON WITH BASE

The main goal of BASE was to improve understanding of weather systems in the Arctic during the fall season. BASE was conducted from September 19 through October 29, 1994 in the Beaufort Sea, north of the mouth of the Mackenzie River. The principal data set was obtained from the National Center for Atmospheric Research (NCAR) C-130 aircraft. There were 14 research flights with the duration of 6 to 8 hours each. These flights have provided large volumes of data covering a wide range of SBL and sea ice conditions. The description of the data can be found in Curry et al. (1996). In this study, the soundings of wind and temperature, collected during flight 7 (73 N, 133 W) over a frozen sea surface, were used. No clouds were present while the potential temperature profile ensured strong stable stratification. The soundings extended down to the altitude of 40 *m* where the temperature could be as low as -12.5°C yet the well-mixed surface layer could not be reached. The surface temperature of the frozen sea was about -15°C (corresponding to 257°K at pressure of 1013 *mb*) suggesting that stable stratification could extend all the way down to the surface. The extrapolation of the potential temperature Θ from the lowest 100 *m* of the sounding to the surface yields $\frac{\partial\Theta}{\partial z} \sim 0.057^{\circ}\text{K m}^{-1}$ which corresponds to the Brunt-Väisälä frequency $N \sim 0.046\text{s}^{-1}$ (Paluch and Lenschow, 1997). Note that the frozen sea surface in flight 7 was not uniform as it included open leads. Since the larger leads extended over several hundred meters and the aircraft flew only about 40 *m* above the surface, it was expected that the aircraft would encounter warm and moist plumes rising from the leads. However, the data from flight 7 showed no signature of such plumes. The data from flight 7 of BASE was successfully simulated in LES by Kosovic and Curry (2000) who considered two cases, NLHRB and NLMR10CR. The difference between the cases was in the rate of the surface cooling equal to $0.25^{\circ}\text{K hr}^{-1}$ in the first case, which was a moderately stable ABL, and $1.0^{\circ}\text{K hr}^{-1}$ in the second case, which was a strongly stable ABL. Thus, the BASE data covered the two extreme cases mentioned in the Introduction. The strength of the overlying inversion was $0.01^{\circ}\text{K m}^{-1}$ and the surface roughness was 0.1 *m*. In the LES, the transitional process of the boundary layer adjustment to the respective surface cooling rates was simulated for each of the two cases.

Using the new $K-\epsilon$ model, we have simulated the same experiments in a single-column formulation with the vertical resolution of 10 *m*. The boundary conditions for the turbulence characteristics at the first grid point are: $K = 3.75u_*^2$, $\epsilon = u_*^3/\kappa z$, $-\overline{uw} = C_D|\mathbf{U}|U$, $-\overline{vw} = C_D|\mathbf{U}|V$, $-\overline{\theta w} = C_H|\mathbf{U}|(\Theta_1 - \Theta_s)$. Here, $\kappa = 0.4$ is the von-Karman

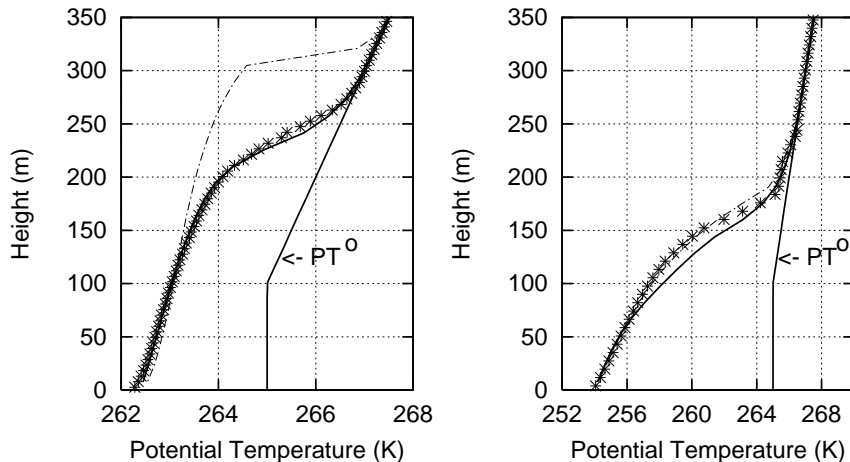


Figure 5. Vertical profiles of mean potential temperature for the cases of moderate (left panel) and strong (right panel) stable stratification simulated with the new (solid line) and the standard (dashed-dotted line) $K - \epsilon$ models. The LES results by Kosovic and Curry (2000) are shown by asterisks. The initial PT profiles (marked as PT^0) are shown by straight solid lines.

constant, z is the distance to the surface, C_D and C_H are the drag and the heat transfer coefficients, $|\mathbf{U}|$ is the magnitude of the near-surface wind, Θ_1 and Θ_s are the PT values at the first grid point and at the surface, respectively. The C_D and C_H coefficients include correction due to the PT gradient outside of the boundary layer (Zilitinkevich and Calanca, 2000; Zilitinkevich et al., 2002b). At the upper boundary, zero values of K , ϵ , heat and momentum fluxes are set. Both cases of the moderate and strong stratification were simulated for 12 hours of physical time during which the flow attained a quasi-steady state. The initial values of the turbulent kinetic energy and dissipation were set equal to small constants. In the course of the simulations, the model “forgot” the initial distributions of K and ϵ after, approximately, one hour of integration.

Figure 5 shows the profiles of the potential temperature (PT) simulated with the new and the standard $K - \epsilon$ models as well as with the LES after 12 hours simulation. The agreement of the new model with the LES data is very good for the case of moderate stratification. The standard model strongly overestimates the height of the temperature boundary layer in that case. In the case of strong stratification, the simulated temperature profile is lower than in LES. In order to understand the source of this discrepancy, recall that the SGS viscosities and diffusivities in LES by Kosovic and Curry (2000) were adopted

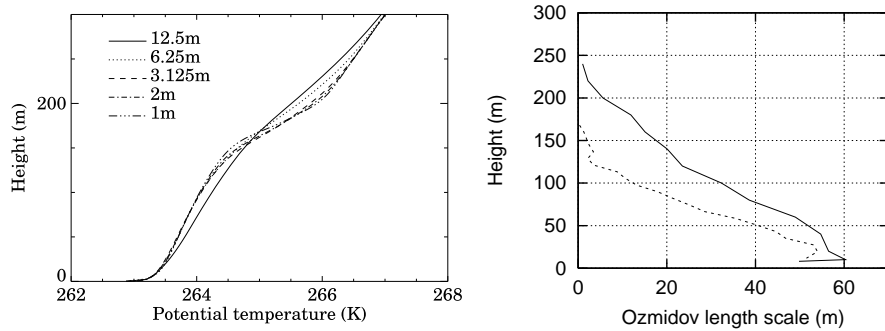


Figure 6. Left panel: mean PT profiles at different grid resolutions (the resolutions are shown in the top left corner of the panel) for the final hour of UK Meteorological Office simulations of BASE data with moderate stable stratification (courtesy of Robert Beare, UK Met Office); right panel: vertical profiles of the Ozmidov length scale L_O obtained from LES by Kosovic and Curry (2000) after 12 hours of simulated time (solid and dashed lines refer to the cases of moderate and strong stratification, respectively).

from the neutral case thus ignoring the effect of stable stratification on SGS parameters. As discussed earlier, such an approximation is justified when the grid size is smaller than the Ozmidov length scale, $L_O = \pi/k_O$. However, in strong stratification, L_O decreases and may become comparable to or even smaller than the grid size. As evident from Fig. 1, eddy viscosities and diffusivities in this case are significantly reduced compared to their values in neutral stratification. The use of the latter in strongly stratified flows may result in overestimated mixing and overpredicted boundary layer height. Since the eddy diffusivity in such flows decreases much faster than the eddy viscosity, the overprediction of the temperature boundary layer height may be most profound. To avoid this problem, one can either increase the grid resolution or account for the effect of stratification on SGS parameters. Figure 6 substantiates these arguments. The left panel shows profiles of potential temperature for the moderately stratified case of BASE after 9 hours of simulated time computed in LES with variable grid resolution; the model of the UK Meteorological Office has been employed in this LES. One can see that indeed, the increase in resolution is accompanied by the lowering of the PT profiles and sharpening of their gradients. The right panel shows the vertical profiles of the Ozmidov scale for moderate and strong stable stratification calculated from the data in LES by Kosovic and Curry (2000). In the case of the moderate stratification, the grid resolution was 5.51 m; L_O remained well above this value almost everywhere except for the top of the boundary layer such that the

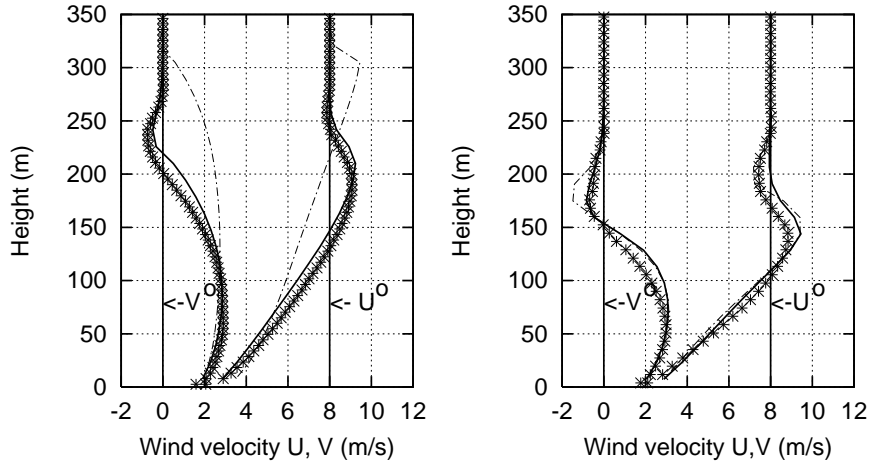


Figure 7. Vertical profiles of mean horizontal wind components, U and V , simulated with the new and the standard $K - \epsilon$ models. The initial profiles are marked as U^0 and V^0 , respectively. The order of the panels and the description of the lines and asterisks are the same as in Fig. 5.

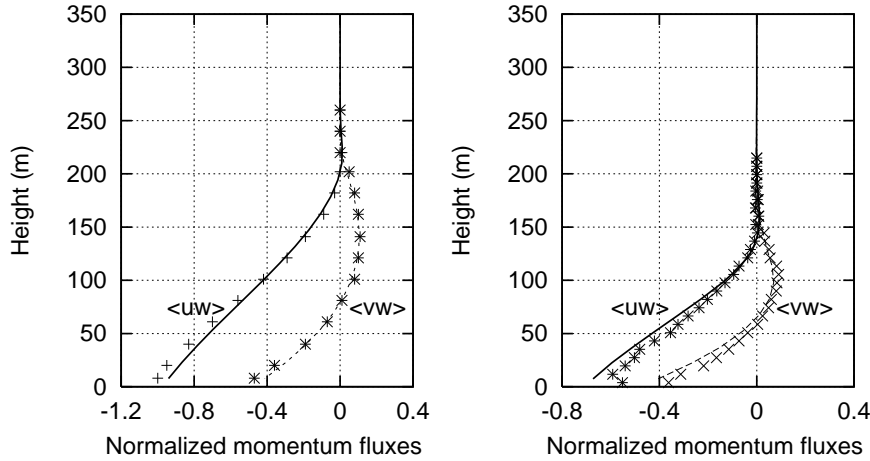


Figure 8. Normalized vertical momentum fluxes for the cases of moderate (left panel) and strong (right panel) stable stratification. Discrete data are from LES by Kosovic and Curry (2000), lines are from the new $K - \epsilon$ model.

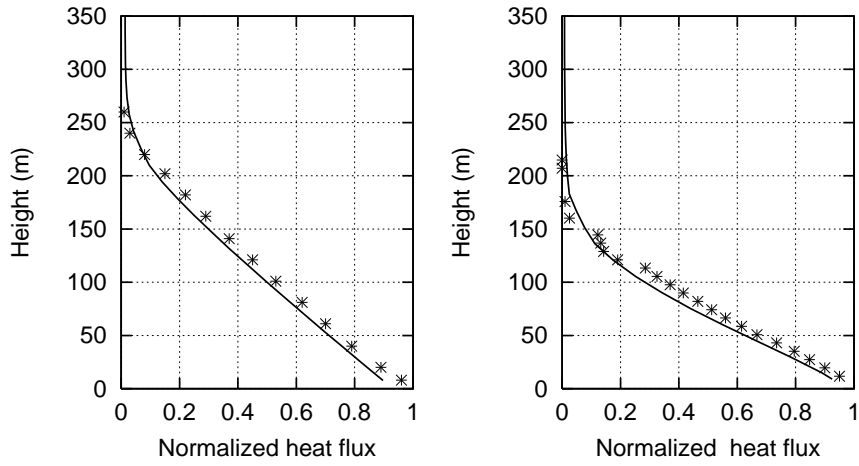


Figure 9. Normalized vertical heat flux. The description of the panels and the data is the same as in Fig. 8

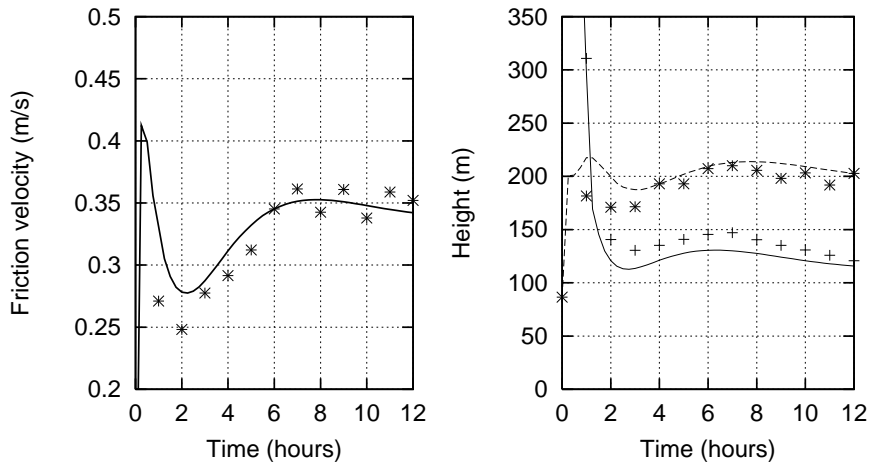


Figure 10. Friction velocity, u_* , (solid line; left panel) and Monin-Obukhov length scale and boundary layer height (solid and dashed lines, respectively; right panel) obtained with the new $K - \epsilon$ model and LES by Kosovic and Curry (2000) (asterisks and crosses). Both panels refer to the case of moderately stable stratification.

neutral stratification-based SGS parameters used in Kosovic and Curry (2000) could be expected to yield a satisfactory performance. Indeed, Kosovic and Curry (2000) report a good agreement between their LES and the observational data. On the other hand, in the strongly stratified case, L_O becomes comparable to the grid size (equal to $7.81m$) already at the heights of about $100 m$ such that the effect of stratification on the SGS parameters cannot be neglected. The discrepancy between LES results of Kosovic and Curry (2000) and the present model shown in Fig. 5 at the heights of about $100 m$ and above can, most probably, be attributed to the fact that the SGS parameterization in LES did not account for the effect of stable stratification. To fully resolve this important issue, more detailed observational and experimental studies of boundary layers with strong stable stratification are required.

The vertical profiles of the horizontal wind components, U and V , are shown in Fig. 7. The results obtained with the new $K-\epsilon$ model show good agreement with the LES-generated wind profiles. The standard $K-\epsilon$ model does not perform well in the case of the moderate stratification but under strong stratification its performance is significantly improved.

Profiles of the vertical turbulent momentum and heat fluxes are compared with LES by Kosovic and Curry (2000) on Figs. 8 and 9. The agreement is close for both moderate and strong stable stratification.

The important integral characteristics of SBLs are the friction velocity u_* , the Monin-Obukhov length scale, L_{MO} , and the boundary layer height h (defined as a level at which the turbulent momentum flux falls to 5% of its surface value) shown on Fig. 10 for the case of moderately stable stratification. One can see that the evolution of all three parameters is faithfully replicated by the $K-\epsilon$ model.

4.2. COMPARISON WITH SHEBA DATA

The Surface Heat Budget of the Arctic Ocean (SHEBA) experiment consists of an array of instrument sites arranged around an icebreaker frozen in the Arctic Ocean pack ice (Uttal et al., 2002; Andreas et al., 1999). The entire field camp drifted together with the pack ice across the Beaufort and Chukchi seas during the year, approximately 1500 km. A lot of atmospheric and surface data were recorded along this course. One of the main objectives of the SHEBA experiment was to collect surface and atmospheric boundary layer data suitable for evaluation of parameterization schemes of ABL employed in global circulation and numerical weather prediction models for high latitudes. The data used in the present study were obtained from two measurement platforms, the Atmospheric Surface Flux Group (ASFG) and the GPS/Loran At-

mospheric Sounding System. The ASFG site consisted of a 20 meters height tower with meteorological sensors at five levels above the surface, as well as several ground based measurement platforms surrounding the tower. The ASFG data included the surface pressure, temperature, sensible and latent heat fluxes, wind stress and albedo, and vertical profiles of temperature and wind velocity in the lowest twenty meters of the ABL (Persson et al., 2002). The vertical profiles of temperature, humidity and winds above the ASFG tower were obtained with the Väisälä radiosondes which were launched from the ship deck. In the present study, we used data from the winter case of 15 January, from 0 to 12 hours. The values of temperature and velocity components above the tower at 12 hours were obtained by linear interpolation between launch times. In the vertical, all radiosonde data values at each height above the ASFG tower were smoothed using six-point running mean values. At initial time, which for the winter case of 15 January was characterized by strong stability, low surface temperature was $T_s = 235^\circ K$ and the geostrophic wind velocity was $U_g = 6 \text{ m s}^{-1}$. During 12 hours, U_g increased to 8.2 m s^{-1} and T_s decreased to $233.5^\circ K$. This process was simulated using the new $K - \epsilon$ model in a single-column format; the results of 12 hour integration are shown in Fig. 11. The observed vertical profile of potential temperature above ABL had shifted during the integration period relative to the initial profile. The analysis of the ECMWF weather forecast for this period has shown a week subsidence (negative vertical velocity) over the area of study. To reflect the ensuing processes of the large-scale vertical advection of potential temperature and velocity, a negative vertical velocity of $-10^{-3} \text{ m s}^{-1}$ was incorporated in the model. With vertical advection accounted for, the simulated potential temperature and velocity profiles are in good agreement with the observational data. On the other hand, Fig. 11 shows that the data cannot be reliably reproduced if the vertical advection is not accounted for.

5. Discussion and conclusions

The spectral theory of turbulence employed in this study is based upon a process of successive elimination of small scale modes that leads to a model describing the largest scales of a flow. Partial scale elimination can be used to derive turbulent viscosities and diffusivities suitable for SGS parameterization in LES. The elimination of all scales leads to RANS-type models. The spectral model is derived from first principles and is free of empirical coefficients. The model yields a dispersion relation for internal waves in presence of turbulence and offers a powerful

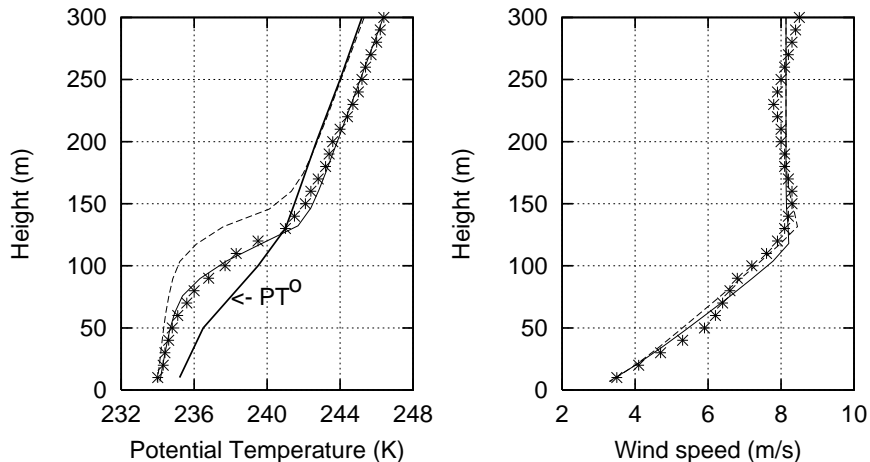


Figure 11. Vertical profiles of potential temperature (left panel) and wind speed (right panel) in SHEBA experiment. The observational data is represented by asterisks, the simulations are shown by the thin solid lines. The short dashed lines refer to the case in which the vertical advection is not accounted for.

tool to study wave-turbulence interaction. The model recognizes the horizontal-vertical anisotropy introduced by stable stratification and provides expressions for the horizontal and vertical turbulent viscosities and diffusivities. The theory does not support an idea of a sharp cut-off critical Richardson number at which turbulence is fully inhibited. Instead, it predicts a transitional range of Ri in which vertical mixing is suppressed while the horizontal mixing is enhanced. The vertical turbulent viscosities and diffusivities obtained in the RANS mode (averaging over all scales) can be used in a $K - \epsilon$ model. The modification of the coefficient C_1 in the ϵ -equation to include the effect of stable stratification results in a general $K - \epsilon$ model suitable for applications in engineering flows as well as in neutral and stably stratified ABLs. This is a significant improvement in the $K - \epsilon$ modeling. The new $K - \epsilon$ model has been tested in simulations of SBLs over sea ice under the conditions of moderate and strong stable stratification. The predicted potential temperature and wind velocity, as well as the friction velocity, the Monin-Obukhov length scale and the boundary layer height are in good agreement with the corresponding values obtained in LES of BASE (Kosovic and Curry, 2000) in the case of moderately stable stratification. In the case of strong stratification, the predicted potential temperature appears to slightly deviate from the LES results in the upper part of the SBL. The source of this discrepancy has been traced to the use of the SGS parameterization in the LES suitable

for the neutrally stratified flows. The measure of deviation of the SGS viscosities and diffusivities from their values under neutral stratification is the ratio, k_c/k_O , where k_c and k_O are the grid resolution and the Ozmidov wave numbers, respectively. When $k_c/k_O = O(1)$, the effect of stable stratification on the SGS parameterization must be accounted for. Indeed, the part of the SBL where the LES and the present results differ coincides with the region where that ratio is $O(1)$. Additional experimental and/or observational data for such situations is necessary to fully resolve this complicated problem. Finally, the profiles of the mean potential temperature and wind speed predicted by the new $K - \epsilon$ model are in very good agreement with the observational data from SHEBA (Uttal et al., 2002).

This paper presents only one of the first attempts to test and validate the new spectral closure-based $K - \epsilon$ model; further comparisons with experimental and observational data as well as with DNS and LES results are clearly needed. However, one can already see that the new technique appears promising for practical applications and can be beneficial if implemented in multi-dimensional circulation models.

Acknowledgements

The authors are thankful to Robert Beare from the UK Met Office for providing the left panel of Fig. 6 and to two anonymous reviewers for constructive suggestions. Support of this research by the ARO grant DAAD19-01-1-0816, the Israel Science Foundation grant No. 134/03, EU project “Integrated Observing and Modelling of the Arctic Sea Ice and Atmosphere (IOMASA)” - EVK3-CT-2002-00067, and Swedish Meteorological and Hydrological Institute (SMHI) EU INTAS project “Representation of lakes in numerical models for environmental application” is greatly appreciated.

Appendix

A. Asymptotic cases of weak and strong stable stratification

It is convenient to introduce a spectral Froude number,

$$\mathcal{F} \equiv \frac{\nu_h k^2}{N}, \quad (27)$$

that measures the ratio of the internal wave period to the turbulence turnover time of the mode k . The asymptotic cases of $\mathcal{F} \rightarrow \infty$ and

$\mathcal{F} \rightarrow 0$ correspond to weak and strong stratification, respectively. In these two cases, the expressions for $R_1 - R_4$ simplify significantly; they are presented below.

B. Case of weak stratification, $\mathcal{F} \rightarrow \infty$

A small parameter expansion in powers of \mathcal{F}^{-1} yields, in the lowest order approximation,

$$R_1 = \frac{1}{5 \nu_h^2} + \mathcal{F}^{-2} \left[\frac{-1}{70 \kappa_h \nu_h} - \frac{2 \kappa_h}{105 (\kappa_h + \nu_h)^3} + \frac{1}{70 (\kappa_h + \nu_h)^2} + \frac{1}{70 \kappa_h (\kappa_h + \nu_h)} \right] + \frac{\nu_h - \nu_z}{5 \nu_h^3}, \quad (28)$$

$$R_2 = \frac{1}{5 \nu_h^2} + \mathcal{F}^{-2} \left[\frac{-29}{105 \kappa_h \nu_h} + \frac{8 \kappa_h}{105 (\kappa_h + \nu_h)^3} - \frac{4}{21 (\kappa_h + \nu_h)^2} + \frac{29}{105 \kappa_h (\kappa_h + \nu_h)} \right] + \frac{2 (\nu_h - \nu_z)}{15 \nu_h^3}, \quad (29)$$

$$R_3 = \frac{2}{3 \nu_h (\kappa_h + \nu_h)} \left[1 - \frac{\mathcal{F}^{-2} \nu_h}{10 \kappa_h} + \frac{2 (\kappa_h - \kappa_z)}{5 (\kappa_h + \nu_h)} + \frac{2 (\kappa_h + 2 \nu_h) (\nu_h - \nu_z)}{5 \nu_h (\kappa_h + \nu_h)} \right], \quad (30)$$

$$R_4 = \frac{2}{3 \nu_h (\kappa_h + \nu_h)} \left[1 - \frac{4 \mathcal{F}^{-2} \nu_h}{5 \kappa_h} + \frac{\kappa_h - \kappa_z}{5 (\kappa_h + \nu_h)} + \frac{(\kappa_h + 2 \nu_h) (\nu_h - \nu_z)}{5 \nu_h (\kappa_h + \nu_h)} \right]. \quad (31)$$

C. Case of strong stratification, $\mathcal{F} \rightarrow 0$

In the limit $\mathcal{F} \rightarrow 0$, the following expressions for $R_1 - R_4$ are obtained:

$$R_1 = \frac{1}{64} \left\{ \frac{2}{\nu_h \nu_z} + \frac{1}{-\nu_h^2 + \nu_h \nu_z} \right. \\ + \frac{2 (\kappa_h + \nu_h) (4 \kappa_h + 3 \nu_h) + (22 \kappa_h + 9 \nu_h - 15 \kappa_z - 15 \nu_z) (\kappa_z + \nu_z)}{(\kappa_h + \nu_h - \kappa_z - \nu_z)^3 (\kappa_z + \nu_z)} \\ - \frac{\kappa_z [-2 (\kappa_h + \nu_h)^2 + (\kappa_z + \nu_z) [9 (\kappa_h + \nu_h) + 8 \kappa_z + 8 \nu_z]]}{(\kappa_h + \nu_h - \kappa_z - \nu_z)^3 (\kappa_z + \nu_z)^2} \\ + \operatorname{arcsinh} \sqrt{-1 + \frac{\nu_h}{\nu_z} \frac{4 \nu_h - 3 \nu_z}{[\nu_h (\nu_h - \nu_z)]^{\frac{3}{2}}}} \\ - \operatorname{arcsinh} \sqrt{-1 + \frac{\kappa_h + \nu_h}{\kappa_z + \nu_z} \sqrt{\frac{\kappa_h + \nu_h}{(\kappa_h + \nu_h - \kappa_z - \nu_z)^5}} \left[\frac{17 \kappa_h + 20 \nu_h + \kappa_z + \nu_z}{\kappa_h + \nu_h} \right. \right.$$

$$+ \left. \frac{15 (\kappa_h - \kappa_z)}{\kappa_h + \nu_h - \kappa_z - \nu_z} \right\}, \quad (32)$$

$$R_2 = \frac{1}{16} \left[\frac{-20 \kappa_h + 2 \kappa_z - 21 \nu_h}{(\kappa_h + \nu_h) (\kappa_h - \kappa_z + \nu_h - \nu_z)^2} + \frac{\kappa_h + 2 \kappa_z + \nu_h}{(\kappa_h + \nu_h)^2 (\kappa_h - \kappa_z + \nu_h - \nu_z)} \right. \\ \left. + \frac{2 \kappa_z}{(\kappa_h + \nu_h)^2 (\kappa_z + \nu_z)} + \frac{15 (\kappa_h - \kappa_z)}{(-\kappa_h + \kappa_z - \nu_h + \nu_z)^3} \right] \\ + \frac{\operatorname{arcsinh} \sqrt{-1 + \frac{\kappa_h + \nu_h}{\kappa_z + \nu_z}}}{16 \sqrt{(\kappa_h + \nu_h) (\kappa_h - \kappa_z + \nu_h - \nu_z)}} \left[\frac{-1}{\kappa_h + \nu_h} + \frac{15 (\kappa_h - \kappa_z) (\kappa_h + \nu_h)}{(\kappa_h - \kappa_z + \nu_h - \nu_z)^3} \right. \\ \left. + \frac{3 (5 \kappa_h + \kappa_z + 7 \nu_h)}{(\kappa_h - \kappa_z + \nu_h - \nu_z)^2} + \frac{9 \kappa_h + 8 \nu_h}{(\kappa_h + \nu_h) (-\kappa_h + \kappa_z - \nu_h + \nu_z)} \right], \quad (33)$$

$$R_3 = \frac{\sqrt{1 - \frac{\nu_z}{\nu_h}} \operatorname{arcsinh} \sqrt{-1 + \frac{\nu_h}{\nu_z}} - \sqrt{1 - \frac{\kappa_z + \nu_z}{\kappa_h + \nu_h}} \operatorname{arcsinh} \sqrt{-1 + \frac{\kappa_h + \nu_h}{\kappa_z + \nu_z}}}{2 (\nu_h \kappa_z - \kappa_h \nu_z)}, \quad (34)$$

$$R_4 = O(\mathcal{F}^2). \quad (35)$$

References

- Abarbanel, H.D., Holm, D.D., Marsden, J.E. and Ratiu, T.: 1984, ‘Richardson number criterion for the nonlinear stability of three-dimensional stratified flow’, *Phys. Rev. Lett.* **52**, 2352–2355.
- Andreas, E.L., Fairall, C.W., Guest, P.S. and Persson, P.O.G.: 1999, ‘An overview of the SHEBA atmospheric surface flux program. *13th Symposium on Boundary Layers and Turbulence*, Dallas, TX, Amer. Meteorol. Soc., 550–555.
- Cane, M.: 1993, ‘Near-surface mixing and the ocean’s role in climate’, in: *Large Eddy Simulation of Complex Engineering and Geophysical Flows*, B. Galperin and S.A. Orszag, eds. Cambridge University Press, 489–509.
- Cheng, Y., Canuto, V.M. and Howard, A.M.: 2002, ‘An improved model for the turbulent PBL’, *J. Atmos. Sci.* **59**, 1550–1565.
- Cho, J.Y.N., Newell, R.E. and Barrick, J.D.: 1999, ‘Horizontal wavenumber spectra of winds, temperature, and trace gases during the Pacific Exploratory Missions: 2. Gravity waves, quasi-two-dimensional turbulence, and vortical modes’, *J. Geophys. Res.* **104**, 16297–16308.
- Curry, J.A.: 1986, ‘Interaction among turbulence, radiation and microphysics in Arctic stratus clouds’, *J. Atmos. Sci.* **43**, 90–106.
- Curry, J.A., Ebert, E.E. and Herman, G.F.: 1988, ‘Mean and turbulence structure of the summertime Arctic cloudy boundary layer’, *Quart. J. R. Meteorol. Soc.* **114**, 715–746.
- Curry, J.A., Rossow, W.B., Randall, D. and Schramm, J.L.: 1996, ‘Overview of Arctic cloud and radiation characteristics’, *J. Climate* **9**, 1731–1764.
- Detering, H. and Etling, D.: 1985, ‘Application of the $E-\epsilon$ model to the atmospheric boundary layer’, *Boundary-Layer Meteorol.* **33**, 113–133.

- Fett, R.W., Burk, S.D. and Thompson, W.T.: 1994, 'Environmental phenomena of the Beaufort sea observed during the Leads Experiment', *Bull. Am. Meteorol. Soc.* **75**, 2131–2145.
- Galperin, B., Kantha, L.H., Hassid, S. and Rosati, A.: 1988, 'A quasi-equilibrium turbulent energy model for geophysical flows', *J. Atmos. Sci.* **45**, 55–62.
- Galperin, B. and Kantha, L.H.: 1989, 'Turbulence model for rotating flows', *AIAA J.* **27**, 750–757.
- Galperin, B. and Mellor, G.L.: 1991, 'The effects of streamline curvature and spanwise rotation on near-surface, turbulent boundary-layers', *J. Appl. Math. and Physics (ZAMP)* **42**, 565–583.
- Galperin, B. and Orszag, S., Eds. 1993: *Large Eddy Simulation of Complex Engineering and Geophysical Flows*, Cambridge University Press, 622pp.
- Galperin, B., Rosati, A., Kantha, L.H. and Mellor, G.L.: 1989, 'Modeling rotating stratified turbulent flows with application to oceanic mixed layers', *J. Phys. Oceanogr.* **19**, 901–916.
- Hahn, C.J., Warren, S.G., London, J., Chervin, R.M., and Jenne, R.L.: 1984, 'Atlas of simultaneous occurrences of different cloud types over land', *NCAR Tech. Note TN-241-STR*, 21 pp.
- Holtslag, A.A.M.: 2003, 'GABLS initiates intercomparison for stable boundary layer case', *GEWEX News* **13**, 7–8.
- Howard, L. N.: 1961, 'Note on a paper of John W. Miles', *J. Fluid Mech.* **10**, 509–512.
- Huschke, R.E.: 1969, 'Arctic cloud statistics from air-calibrated surface weather observations', *The Rand Corporation RM-6173-PR*, 79 pp.
- Intrieri, J.M., Shupe, M.D., Uttal, T., and McCarty, B.J.: 2002, 'Annual cycle of Arctic cloud geometry and phase from radar and lidar at SHEBA', *J. Geophys. Res.* **107**, 8030.
- Kantha, L.H.: 2003, 'On an improved model for the turbulent PBL', *J. Atmos. Sci.* **60**, 2239–2246.
- Kantha, L.H. and Clayson, C.A.: 1994, 'An improved mixed-layer model for geophysical applications', *J. Geophys. Res.* **99**, 25235–25266.
- Kim, J. and Mahrt, L.: 1993, 'Simple formulation of turbulent mixing in the stable free atmosphere and nocturnal boundary layer', *Tellus* **44A**, 381–394.
- King, J. C.: 1990, 'Some measurements of turbulence over an Antarctic ice shelf', *Quart. J. Roy. Meteorol. Soc.* **116**, 379–400.
- Kitaigorodskii, S. A. and Joffe, S. M.: 1988, 'In search of simple scaling for the heights of the stratified atmospheric boundary layer', *Tellus* **40A**, 419–443.
- Kondo, J., Kanechika, O. and Yasuda, N.: 1978, 'Heat and momentum transfer under strong stability in the atmospheric surface layer', *J. Atmos. Sci.* **35**, 1012–1021.
- Kosovic, B. and Curry, J.A.: 2000, 'A large eddy simulation study of a quasi-steady, stably stratified atmospheric boundary layer', *J. Atmos. Sci.* **57**, 1052–1068.
- Kraichnan, R.H.: 1959, 'The structure of isotropic turbulence at very high Reynolds numbers', *J. Fluid Mech.* **5**, 497–543.
- Kraichnan, R.H.: 1987, 'An interpretation of the Yaghot-Orszag turbulence theory', *Phys. Fluids* **30**, 2400–2405.
- Large, W.G., J.C. McWilliams, and P. Niiler, 1986: Upper ocean thermal response to strong autumnal forcing of the northeast Pacific. *J. Phys. Oceanogr.*, **16**, 1524–1550.
- Large, W.G., McWilliams, J.C. and S.C. Doney.: 1994, 'Oceanic vertical mixing: A review and a model with nonlocal boundary layer parameterization', *Rev. Geophys.* **32**, 363–403.

- Larsen, S. E., Courtney, M. and Mahrt, L.: 1990, 'Low frequency behaviour of horizontal power spectra in stable surface layers', *Proc. 9th AMS Symposium on Turbulence and Diffusion*, American Meteorological Society, Boston, USA, 401-404.
- Mack, S.A. and H.C. Schoeberlein: 2004, 'Richardson number and ocean mixing: Towed chain observations', *J. Phys. Oceanogr.* **34**, 736–754.
- Mahrt, L.: 1998, 'Stratified atmospheric boundary layers and breakdown of models', *Theoret. Comput. Fluid Dyn.* **11**, 263–279.
- Mahrt, L.: 1999, 'Stratified atmospheric boundary layers', *Boundary-Layer Meteorol.* **90**, 375–396.
- McComb, W.D.: 1991, 'The Physics of Fluid Turbulence', *Oxford University Press*, 576 pp.
- Mellor, G.L. Yamada, T.: 1982, 'Development of turbulence closure model for geophysical fluid problems', *Rev. Geophys. Space Phys.* **20**, 851–875.
- Miles, J. W.: 1961, 'On the stability of heterogeneous shear flows', *J. Fluid Mech.* **10**, 496-508.
- Orszag, S.A.: 1977, 'Statistical theory of turbulence', in *Les Houches Summer School in Physics*, R. Balian and J.-L. Peabe, eds. Gordon and Breach, 237-374.
- Paluch, I.R. and Lenschow, D.H.: 1997, 'Arctic boundary layer in the fall season over open and frozen sea', *J. Geophys. Res.*, **102**, 25955–25971.
- Perov, V., Zilitinkevich, S. and Ivarsson, K.-I.: 2001, 'Implementation of new parameterisation of the surface turbulent fluxes for stable stratification in the 3-D HIRLAM', *HIRLAM Newsletter*, *37*, 60–66.
- Persson, P.O.G., Fairall, C.W., Andreas, E.L., Guest, P.S. and Perovich, D.K.: 2002, "Measurements near the atmospheric surface flux group tower at SHEBA: Site description, data processing and accuracy estimates", *NOAA Tech. Memo. OAR ETL*.
- Perov, V. and Gollvik, S.: 1996, 'A 1-D test of a non-local $K - \epsilon$ boundary layer scheme for a NWP model resolution', *HIRLAM Technical Report* **25**.
- Peters, H., Gregg, M.C. and Toole, J.M.: 1988, 'On the parameterization of equatorial turbulence', *J. Geophys. Res.* **93**, 1199–1218.
- Pinto, J.O. and Curry, J.A.: 1995, 'Atmospheric convective plumes emanating from leads, II, Microphysical and radiative processes', *J. Geophys. Res.* **100**, 4633–4642.
- Ramanathan, V., Cess, R.D., Harrison, E.F., Minnis, P., Barkstrom, B.R., Ahmad, E. and Hartman, D.: 1989, 'Cloud radiative forcing and climate: Results from the Earth Radiative Budget Experiment', *Science* **243**, 63–67.
- Rodi, W., 1975: 'A note on the empirical constant in the Kolmogorov-Prandtl eddy-viscosity expression', *J. of Fluids Eng.*, Trans. ASME, 386–389.
- Rodi, W.: 1980, 'Turbulence models and their application in hydraulics', *Tech. Rep.* Int. Assoc. for Hydraul. Res., Delft, Netherlands.
- Rossow, W.B., Walker, A.W. and Garder, L.C.: 1993, 'Comparison of ISCCP and other cloud amounts', *J. Climate* **6**, 2394-2418.
- Ruffeaux, D., Ola, P., Persson, G., Fairall, C. and Wolfe, D.E.: 1995, 'Ice pack and surface energy budgets during LEADDEX 1992', *J. Geophys. Res.* **100**, 4593-4612.
- Sukoriansky, S. and Galperin, B.: 2004, 'A spectral closure model for turbulent flows with stable stratification', in: *Marine Turbulence - Theories, Observations and Models*, H. Baumert, J. Simpson, J. Sundermann, eds., Cambridge University Press, in press.
- Sukoriansky, S., Galperin, B., and Staroselsky, I.: 2003, 'Cross-term and ϵ -expansion in RNG theory of turbulence', *Fluid Dyn. Res.* **33**, 319–331.

- Tsay, S.C. and Jayaweera, K.: 1984, 'Physical characteristics of Arctic stratus clouds', *J. Clim. Appl. Meteorol* **23**, 584–596.
- Uttal T. et al.: 2002, 'Surface heat budget of the Arctic Ocean', *Bull. Amer. Met. Soc.* **83**, 255–276.
- Walter, B.A., Overland, J.E. and Turet, P.: 1995, 'A comparison of satellite-derived and aircraft-measured surface sensible heat fluxes over the Beaufort Sea', *J. Geophys. Res.* **100**, 4583–4591.
- Yakhot, V. and Orszag, S.A.: 1986, 'Renormalization group analysis of turbulence. I. Basic theory', *J. Sci. Comput.* **1**, 3–51.
- Zilitinkevich, S.: 2002, 'Third-order transport due to internal waves and non-local turbulence in the stably stratified surface layer', *Quart. J. Roy. Met. Soc.* **128**, 913–925.
- Zilitinkevich, S.S., Baklanov, A., Rost, J., Smedman, A.-S., Lykosov, V., and Calanca, P.: 2002a, 'Diagnostic and prognostic equations for the depth of the stably stratified Ekman boundary layer', *Quart. J. Roy. Met. Soc.* **128**, 25–46.
- Zilitinkevich, S.S. and Baklanov, A.: 2002, 'Calculation of the height of stable boundary layers in practical applications', *Boundary-Layer Meteorol.* **105**, 389–409.
- Zilitinkevich, S.S. and Calanca, P.: 2000, 'An extended similarity - theory for the stably stratified atmospheric surface layer', *Quart. J. R. Meteorol. Soc.* **126**, 1913–1923.
- Zilitinkevich S. S. and Esau, I. N.: 2002, 'On integral measures of the neutral, barotropic planetary boundary layers', *Boundary-Layer Meteorol.* **104**, 371–379.
- Zilitinkevich S. S. and Esau, I. N.: 2003, 'The effect of baroclinicity on the depth of neutral and stable planetary boundary layers', *Quart. J. Roy. Met. Soc.* **129**, 3339–3356.
- Zilitinkevich, S. and Mironov, D. V.: 1996, 'A multi-limit formulation for the equilibrium depth of a stably stratified boundary layer', *Boundary-Layer Meteorol.* **81**, 325–351.
- Zilitinkevich, S.S., Perov, V.L., and King, J.C.: 2002b, 'Near-surface turbulent fluxes in stable stratification: Calculation techniques for use in general-circulation models', *Quart. J. R. Meteorol. Soc.* **128**, 1571–1587.

